Optical detection and storage of entanglement in plasmonically coupled quantum-dot qubits

M. Otten,[1,*] S. K. Gray,[1,†] and G. V. Kolmakov[2,‡]
[1]*Center for Nanoscale Materials, Argonne National Laboratory, Argonne, Illinois 60439, USA*
[2]*New York City College of Technology, City University of New York, Brooklyn, New York 11201, USA*

(Received 23 April 2018; published 25 March 2019)

Recent proposals and advances in quantum simulations, quantum cryptography, and quantum communications substantially rely on quantum entanglement formation. Contrary to the conventional wisdom that dissipation destroys quantum coherence, coupling with a dissipative environment can also generate entanglement. We consider a system composed of two quantum-dot qubits coupled with a common, damped surface plasmon mode; each quantum dot is also coupled to a separate photonic cavity mode. Cavity quantum electrodynamics calculations show that upon optical excitation by a femtosecond laser pulse, entanglement of the quantum-dot excitons occurs, and the time evolution of the $g^{(2)}$ pair correlation function of the cavity photons is an indicator of the entanglement. We also show that the degree of entanglement is conserved during the time evolution of the system. Furthermore, if coupling of the photonic cavity and quantum-dot modes is large enough, the quantum-dot entanglement can be transferred to the cavity modes to increase the overall entanglement lifetime. This latter phenomenon can be viewed as a signature of entangled, long-lived quantum-dot exciton-polariton formation. The preservation of total entanglement in the strong-coupling limit of the cavity–quantum-dot interactions suggests a novel means of entanglement storage and manipulation in high-quality optical cavities.

DOI: 10.1103/PhysRevA.99.032339

I. INTRODUCTION

In the past decade, rapid developments in quantum cryptography, quantum communications, and quantum simulations (Refs. [1–3] and references therein) have been made. Interesting examples include the reported low-Earth-orbit satellite-to-ground quantum state transmission [4] that paves the route to a secure "quantum internet," a hundred-kilometer-long optical line for quantum key distribution [5,6], and a publicly available 20-qubit universal quantum computer [7]. These and other advances are stimulating further research into systems that can provide physical realizations of quantum entangled states [8,9]. Previously proposed techniques include coupled quantum rings [10], quasi-phase-matching ring crystals for entangled photon generation [11], and subradiant Dicke states of trapped interacting atoms [12,13]. Recently, a solid-state realization of trapped atoms—coupled quantum-dot (QD) qubits, or "artificial molecules," in a dissipative environment—has been proposed to provide entanglement among electron-hole excitations in QDs (i.e., excitons) in two- and multidot systems at liquid helium temperatures [14–18]. These predictions, still to be validated experimentally, potentially open a new route to the design of robust solid-state emitters of entangled photons of relevance to quantum information science and sensing [19–21].

Some time ago Burkard, Loss, and DiVincenzo [22] proposed coupled quantum dots as a platform for the design of quantum gates, to be used in prospective quantum computers. It is worth noting that the coupled quantum-dot system in high-quality cavity can be mapped into cavity quantum electrodynamics of superconducting electrical circuits [23], which is one of the promising architectures for quantum simulations. Very recently, a programmable two-qubit quantum processor has been realized based on two quantum dots in silicon [24].

It has been found that the second-order correlation function of photons emitted by coupled QD qubits can be utilized as a "witness" of quantum entanglement formation; specifically, antibunching of photons emitted by the QDs has been numerically predicted [25]. Various QD coupling methods have been proposed including sharing the photon field in an optical microcavity [26] or the interactions with auxiliary plasmonic nanoantennas [14–17]. However, direct observations of the entanglement of electronic degrees of freedom in QDs remain challenging.

In this work, we suggest an alternative system for achieving, detecting, and, further, manipulating entanglement of plasmonically coupled QDs in optical microcavities. Specifically, through numerical simulations and theoretical analysis, we demonstrate that, under suitable circumstances, there can be a one-to-one correspondence between the entanglement of QD states and the correlation properties of cavity photons emitted by the QDs. Further, we show that the time dependence of both the QD entanglement and the photon correlation functions is drastically changed from photon correlation suppression or antibunching to strong oscillations during the transition from the weak to strong QD-cavity photon coupling regimes. The latter oscillations are the signature of entangled exciton-polariton states, in which the quantum correlations are shared between the QD excitons and cavity photons. In

*otten@anl.gov
†gray@anl.gov
‡gkolmakov@citytech.cuny.edu

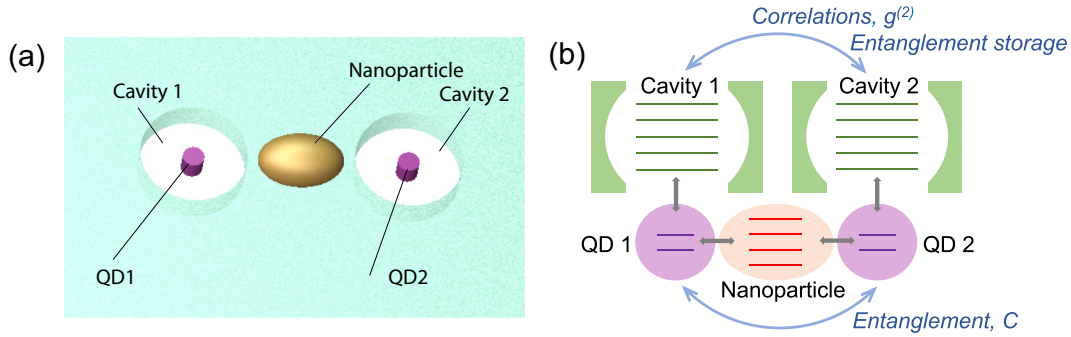

FIG. 1. Schematic of the system. (a) Two quantum-dot (QD) qubits are embedded into optical cavities and coupled with plasmonic modes in a neighboring metal nanoparticle. The chosen setup with two individual cavities, each of them enclosing a single QD, enables one to separately tune the QD-photon and QD-plasmon coupling strengths. (b) Graphical representation of our model: The two-level QDs are coupled with plasmonic modes and photon cavity modes; gray arrows show the respective coupling. In our calculations, the QDs and plasmons are excited by a laser pulse with full width at half maximum of 20 fs. We show that QD qubit entanglement, defined as Wootters' concurrence C, can be both detected via the $g^{(2)}$ pair correlation function of the cavity photon and stored in high-quality optical cavities.

our work, we consider a quantum system driven by a strong femtosecond laser pump. Our results will enable the identification of entanglement in coupled QD systems via cavity photon correlation measurements and also suggest a means of storing such entanglement in the cavity modes.

It is important to note that there is no simple rule—bunching vs antibunching—to be associated with the photon pair correlation function and entanglement or strong coupling and the results will depend on the specific systems and measurements carried out. Here we show, in the system proposed and in the limit of strong coupling between QDs and photonic cavities, that QD entanglement manifests itself as photon *bunching* or sharp peaks in the same-time cross-correlation function for the photons. Thus our results can be contrasted with the steady-state antibunching correlation noted by Dumitrescu and Lawrie [25] that would occur in a quantum-dot–plasmon system without coupling to photonic cavities. The underlying mechanism that leads to the bunching and antibunching behavior in our case is also fundamentally different from that which leads to the bunching behavior predicted for coupled plasmonic systems due to their bosonic character by Masiello and co-workers [27] and the ultrastrong-coupling bunching behavior noted by Savasta and co-workers [28].

II. NUMERICAL MODEL

A. Cavity quantum electrodynamics

A schematic of our system is shown in Fig. 1. The system is composed of two QDs embedded into optical cavities. In addition, the QD electronic degrees of freedom are coupled with the surface plasmon modes in a neighboring metal particle or nanostructure, which provides an efficient dissipative environment. The chosen scheme enables one to controllably and independently tune the QD coupling strengths, compared to the setup where QDs share the same optical cavity. The temporal evolution of the whole system is described by the cavity quantum electrodynamics (CQED) equation for the time-dependent density operator $\hat{\rho}(t)$ [17,29],

$$\frac{\partial\hat{\rho}}{\partial t} = -\frac{i}{\hbar}[\hat{H},\hat{\rho}] - \frac{i}{\hbar}[\hat{H}_d,\hat{\rho}] + L(\hat{\rho}), \tag{1}$$

where $\hat{H} = \hat{H}_0 + \hat{H}_{\rm int}$ is the system Hamiltonian that includes the free Hamiltonians of two ($i = 1, 2$) two-level QDs, surface plasmon, and cavity photon modes,

$$\hat{H}_0 = \sum_i \hbar\omega_i\hat{\sigma}_i^\dagger\hat{\sigma}_i + \hbar\omega_s\hat{b}^\dagger\hat{b} + \sum_i \hbar\omega_i\hat{c}_i^\dagger\hat{c}_i, \tag{2}$$

their interactions,

$$\hat{H}_{\rm int} = -\sum_i \hbar g_s^i(\hat{\sigma}_i^\dagger\hat{b} + \hat{\sigma}_i\hat{b}^\dagger) - \sum_i \hbar g(\hat{\sigma}_i^\dagger\hat{c}_i + \hat{\sigma}_i\hat{c}_i^\dagger), \tag{3}$$

and coupling

$$\hat{H}_d = -E(t)\left[\sum_i d_i(\hat{\sigma}_i + \hat{\sigma}_i^\dagger) + d_s(\hat{b} + \hat{b}^\dagger)\right], \tag{4}$$

with the external driving electromagnetic field $E(t)$ considered in the semiclassical dipole limit (with $\hat{\sigma}_i$, $\hat{b}$, and $\hat{c}_i$ to be the respective annihilation operators for QDs, plasmons, and cavity photon excitations); d_i and d_s are the transition dipole moments of the QDs and plasmons, respectively. We emphasize that the annihilation operators in Eq. (1) act in the coordinate space; thus, whereas the total electron excitation and photon wave functions obey the conventional symmetry dictated by their statistics, their coordinate wave functions can be both symmetric and antisymmetric. The Lindblad superoperator $L(\hat{\rho})$ accounts for the QD and cavity photon population relaxation and dephasing and plasmon dissipation [16,29].

Equation (1) was numerically solved in the rotating-phase approximation with the recently developed "Open quantum systems in C" (QuaC) simulation package [30] based on sparse matrix-vector multiplication algorithms along with the fourth-order Runge-Kutta numerical scheme. We found that the results converged for the number of photon levels $N_{\rm ph} = 4$ and the number of plasmon levels $N_{\rm pl} = 24$. The QD entanglement is captured via Wootters' concurrence $C(t)$ calculated from the QD reduced density matrix [31].

We characterize light in the photonic cavities with the normalized pair correlation function for photons arriving at

the same time [32,33], which in our case simplifies to

$$g_{ij}^{(2)}(t) \equiv g_{ij}^{(2)}(t, \tau = 0) = \frac{\mathrm{Tr}(\hat{c}_i^\dagger \hat{c}_j^\dagger \hat{c}_j \hat{c}_i \hat{\rho}(t))}{n_i(t) n_j(t)}, \qquad (5)$$

where $i, j = 1, 2$ denote the photonic cavity modes, $\hat{c}_i^\dagger$, $\hat{c}_i$ are the corresponding creation and annihilation operators, and $n_i(t) = \mathrm{Tr}(\hat{c}_i^\dagger \hat{c}_i \hat{\rho}(t))$ is the time-dependent population of the ith photon mode.

B. Relevant parameters

In what follows, the QDs are illuminated with a pulsed electric field $E(t) = E_0(t)\cos(\omega t)$, where $E_0(t)$ is a Gaussian envelope function with the maximum electric field of 2.5×10^6 V/m and the full width at half maximum (FWHM) of 20 fs (a fluence of $26.4\,\mathrm{nJ/cm^2}$; see Appendix A). In our simulations we consider low cavity photon mode occupations so that we can disregard renormalization of the photon energies due to nonlinearity [34].

We set the dephasing rate to $8.6\,\mu$eV, corresponding to the temperature 0.1 K. (We note that this temperature is about an order of magnitude higher than that used for superconducting qubits [7].) Equation (1) was numerically solved in the rotating-phase approximation with the recently developed "Open quantum systems in C" (QUAC) simulation package [30] based on sparse matrix-vector multiplication algorithms along with the fourth-order Runge-Kutta numerical scheme. We found that the results converged for the number of photon levels $N_{\mathrm{ph}} = 4$ and the number of plasmon levels $N_{\mathrm{pl}} = 24$.

The photonic cavity environment presents a powerful means for controlling light matter interactions in solid-state systems [35]. Variations in the cavity geometry, the cavity-QD energy detuning, and the QD position relative to the maximum of the light electric field in the cavity and to the plasmonic structure provide an experimental opportunity to alter the QD-cavity photon and QD-surface plasmon interaction strengths in wide limits [36–38]. Furthermore, the use of anisotropic metamaterials as environments for the QDs could provide an additional important tool to manipulate light matter interactions since, as demonstrated by Menon and co-workers, optical topological transitions in these materials significantly modify photon emission rates [39]. The respective QD-photon dimensionless coupling strength $\xi = 4g/(\gamma_{\mathrm{QD}} + \gamma_C)$ varies from $\xi \ll 1$ (weak coupling regime) to ~ 2 (strong coupling) [36,40–42] [with $\gamma_{\mathrm{QD}(C)}$ to be the population relaxation rates for QD excitons (cavity photons)]. The latter value is comparable with $\xi \approx 5$ for single atoms in an optical microcavity [43]. By making use of the Purcell effect, ξ can be further enhanced by an order of magnitude by using high-finesse optical cavities [36,37,44] with quality Q factor $\sim 10^5$. Thanks to the interaction of QDs with overdamped surface plasmons in the neighboring particle, the QD relaxation dominates with the respective decay rate [29] $\gamma_{\mathrm{QD}} = 4g_s^2/\gamma_s > \gamma_C$ (see also Appendix A). Recently, the utility of the strong qubit-photon coupling regimes has been demonstrated for CQED with flux qubits by Armata *et al.* in Ref. [45] where, however, interactions with a strongly dissipative system have not been included.

III. RESULTS AND DISCUSSION

A. Entanglement formation in weak and strong-coupling regimes

We first study the quantum dynamics of a pulsed system (1) in the weak coupling regime for the quantum-dot–photonic cavities. Representative results are shown in Fig. 2 for $\xi = 0.268$. (In the estimate of the respective dimensionless coupling, we use the average $g_s = \frac{1}{2}\sum_{i=1,2} g_s^i$ as the characteristic QD-plasmon interaction strength.) It is seen in the inset of Fig. 2 that the initial QD population oscillations damp at $t \sim 100$ fs after the system is excited by the laser pulse; at later times the QD populations are not equal to each other due to the difference in the QD-plasmon coupling strengths. As the result of this asymmetry, the QD entanglement is formed at $t_C \approx 87$ fs and reaches the maximum $C \sim 0.42$ at $t \approx 220$ fs, as seen in the main plot of Fig. 2 (see Appendix B for more details). It is evident from Fig. 2 that both the cross- and same-cavity correlations $g_{ij}^{(2)}$ of the photons decrease starting from $t \approx t_C$; that is, in the same-time domain where $C(t) > 0$. At later times, $t > 500$ fs, the correlations reach $g_{ij}^{(2)} < 0.1$, corresponding to strong antibunching of the cavity photons. It is worth noting that the time dependence $C(t)$ shown in Fig. 2 is qualitatively similar to that obtained earlier in the simulations in Refs. [16,17] for plasmonically coupled QDs, for which the spontaneous photon emission was described as dephasing in the respective QD Lindblad operator. Thus, we infer that at $\xi \ll 1$, the QD dynamics results in the significant

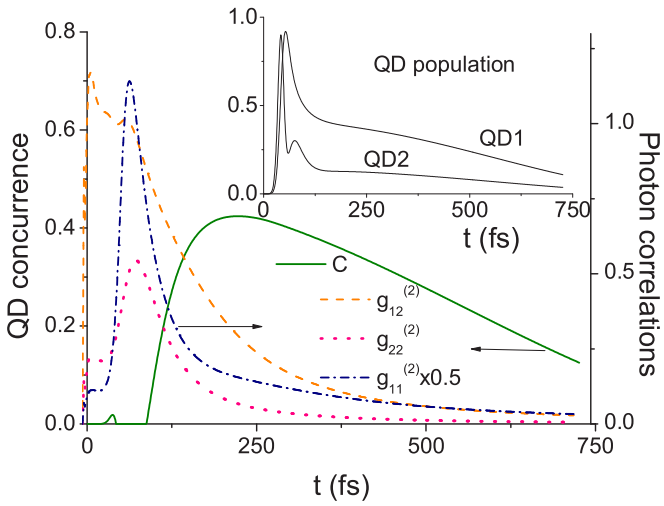

FIG. 2. The dynamics of the system for weak QD-cavity photon coupling, $\xi = 0.268$: QD concurrence $C(t)$ and the same-time cavity photon pair correlation function $g_{ij}^{(2)}(t)$ (main plot), and the QD population (inset). The system is optimally assembled with the QD-plasmon coupling constants ratio of $1/\sqrt{3}$ that maximizes the QD entanglement; $\hbar g_s^i = 30$ and 17.3 meV for $i = 1$ and 2, respectively; $\hbar g = 1$ meV; $\hbar\gamma_s = 150$ meV; the QD decay and dephasing rates are $0.05\,\mu$eV and $8.6\,\mu$eV; the respective photon decay and dephasing rates are 0.1 meV and $8.6\,\mu$eV; the transition dipole moments for the surface plasmons and QDs are $d_s = 4000$ D and $d_i = 13$ D; the energy level spacing of the QD and cavity photon systems is $\hbar\omega = 2.05$ eV (Refs. [16,17,42]). The maximum electric field in the driving pulse is reached at $t = 36.3$ fs.

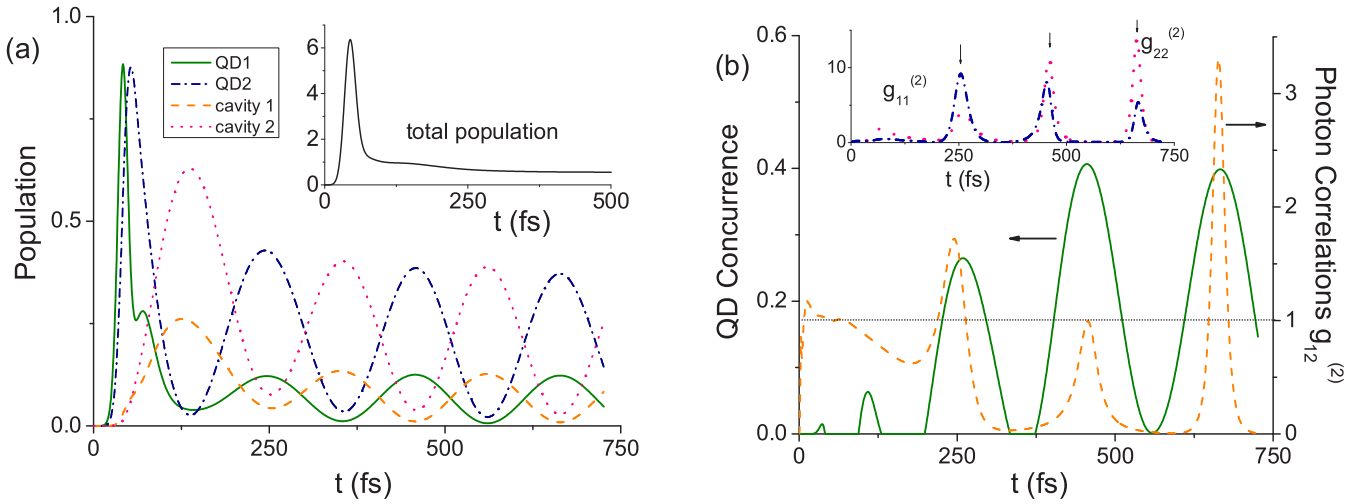

FIG. 3. Oscillatory dynamics of the system in the strong-coupling regime $\xi = 2.68$. (a) Population of QD 1 and 2 and photon population in cavities 1 and 2. Inset shows the total population in the system as a function of time t. (b) QD concurrence and photon correlation functions. Vertical arrows in the inset approximate the moments at which the QD concurrence reaches the maxima, as shown in the main plot. The simulations were done for the same parameters as in Fig. 2, but the QD-cavity photon coupling constant g was increased 10×.

suppression of the cavity photon correlations, whereas the photon dynamics mainly contributes to small QD dephasing rates.

To study the effect of QD-photon interactions on the quantum dynamics of the system, we increased the coupling strength ξ. We found that the results for $\xi > 1$ significantly differ from those obtained above in the weak coupling regime. Figure 3 shows our findings for large coupling $\xi = 2.68$. It is clearly seen in Fig. 3(a) in that, after being excited by the driving pulse at $t \approx 36.3$ fs, both the QD and cavity photon populations exhibit oscillations with the period of $t_0 \approx \pi\hbar/g \approx 217$ fs. However, the total population in the system does not show any significant oscillations [inset in Fig. 3(a)]. The main plot in Fig. 3(b) shows formation and subsequent oscillations of the QD concurrence $C(t)$ that accompanies the population oscillations in Fig. 3(a). It is seen that starting from $t \sim 200$ fs, $C(t)$ reaches maxima at the same times when the QD population builds up.

Figure 3(b) also reveals that, after the initial 150-fs period of relaxation, the cavity photon cross-correlation function $g_{12}^{(2)}(t)$ exhibits oscillations that are synchronous with the QD concurrence oscillations. Specifically, the sharp spikes on the $g_{12}^{(2)}(t)$ curve are positioned at the same moments when $C(t)$ reaches its maxima. The correlation functions $g_{11}^{(2)}(t)$ and $g_{22}^{(2)}(t)$ for the same cavity photon modes follow a similar pattern, as is evident from the inset in Fig. 3(b). Starting from $t \sim 300$ fs, the cavity photons show strong antibunching with $g_{\min}^{(2)} < 0.2$ in time intervals between the maxima. The relative amplitude $k = (g_{\max}^{(2)} - g_{\min}^{(2)})/(g_{\max}^{(2)} + g_{\min}^{(2)})$ of the oscillations reaches $k > 0.9$ that makes it accessible for experimental observations. [Here, $g_{\max(\min)}^{(2)}$ are the maximum (minimum) values of $g_{ij}^{(2)}(t)$ for $i, j = 1, 2$].

The early-time behavior in Fig. 3(b) does not show the interesting correlations between QD concurrence and photon-pair correlation functions. This is because of the nature of the experiment we are imagining that involves an initial pulse exciting the QDs followed by QD-metal particle interaction and entanglement via plasmon interactions. These correlations begin only once a significant concurrence has been established, around 250 fs.

B. Cavity photon entanglement and correlations in the strong-coupling regime

To further understand the effect of the oscillatory dynamics on entanglement, we investigated the correlation properties of the cavity photons. For that purpose, we restricted the number of energy levels of the photon cavity modes in the simulations to $N_{\rm ph} = 2$ for both cavities. This enabled us to determine the entanglement of photons via Wootters' concurrence $C_{\rm ph}(t)$ for the reduced photon density matrix along with the QD concurrence $C(t)$. Our findings are summarized in Fig. 4. It is clearly seen in Fig. 4(a) that, while the concurrence of the photon modes $C_{\rm ph}(t)$ oscillates with time similar to that for QDs in Fig. 3(a), the total concurrence $C_{\rm tot} = C + C_{\rm ph}$ shows a smooth time dependence. In other words, the entanglement is periodically "transferred" between the QD and photon states synchronously with the QD and photon population oscillations, with the total entanglement $C_{\rm tot}$ almost conserved within one oscillation period. We also numerically calculated the fidelity $F(t)$ of the photon states relative to the maximally entangled Bell state Ψ^- that is, to the (antisymmetric) state that mostly contributes to the long-time evolution of the system [17]. It is evident from Fig. 4(a) that after $t > 250$ fs, $F(t)$ oscillates simultaneously with the photon concurrence $C_{\rm ph}(t)$. Thus, $F(t)$ can be viewed as a qualitative characteristic of the photon entanglement. We compared $F(t)$ dependence calculated for $N_{\rm ph} = 2$ with that at $N_{\rm ph} = 4$ (for which our main results were obtained). As is seen in Fig. 4(a), the photon fidelities $F(t)$ for both cases are close to each other. Moreover, it is also evident from Fig. 4(b) that, whereas the photon cross-correlations $g_{12}^{(2)}(t)$ calculated for $N_{\rm ph} = 2$ and 4 are quantitatively different, they show similar qualitative time

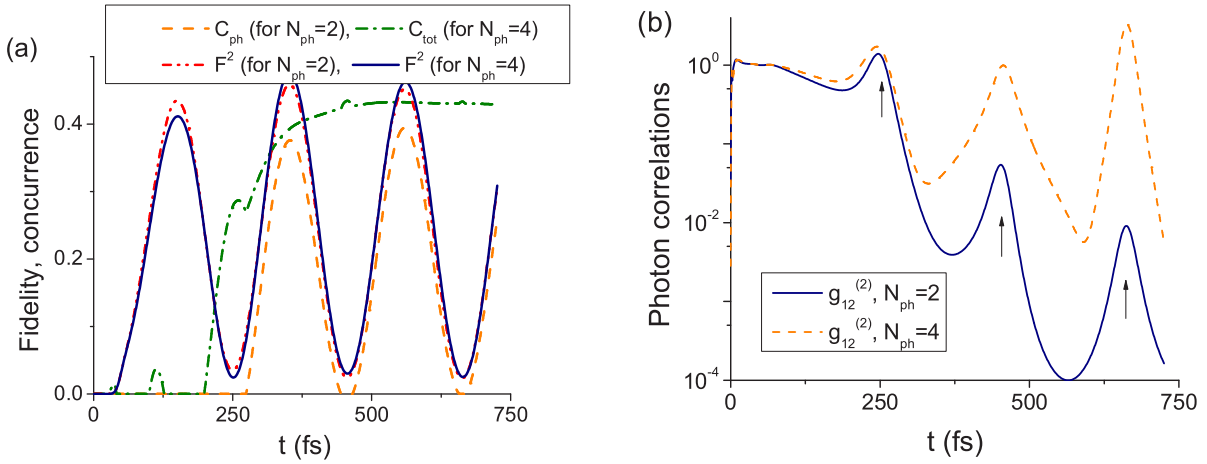

FIG. 4. (a) Photon and total entanglement and (b) the photon cross-correlations for the model where the number of photon levels is restricted to $N_{\rm ph} = 2$. The results are obtained for the strong-coupling regime with the same parameter set as in Fig. 3. It is seen in (a) that the squared fidelity $F^2(t)$ of the photon state relative to the maximally entangled Bell state Ψ^- follows the photon concurrence. It is evident from (a) that change in the photon level number $N_{\rm ph}$ from 2 to 4 does not result to significant changes in fidelity $F(t)$ thus, the photons are entangled at $N_{\rm ph} > 2$. As is also seen in (b), the cross-correlation function $g_{12}^{(2)}$ calculated for $N_{\rm ph} = 2$ and 4 shows similar qualitative patterns with sharp peaks positioned at the moments when the QD entanglement reaches the maximum values in Fig. 3 (arrows).

dependencies with sharp peaks positioned at the moments when the QD entanglement reaches its maximum values (arrows). Therefore, based on the close similarities of the photon fidelities $F(t)$ and the cross-correlation function $g_{12}^{(2)}(t)$ for $N_{\rm ph} = 2$ (for which the concurrence can be explicitly calculated) and $N_{\rm ph} = 4$, we infer that the cavity photon states emerging in the population oscillations are entangled in both cases. We also can say that the $g_{12}^{(2)}(t)$ oscillatory time dependence witnesses the underlying QD entanglement.

It should be noted that the concurrence displayed in Fig. 4(a) is that associated with the photonic modes and so will behave in the opposite manner of the QD concurrence owing to the exchange of entanglement between QD and photonic modes.

The population and entanglement oscillations observed in the strong-coupling regime can be attributed to formation of a correlated QD exciton-cavity photon state, i.e., an exciton polariton. (We will refer to the latter as a polariton.) The polariton state is a quantum superposition of an exciton and a cavity photon, and it has been extensively studied in semiconductor quantum well heterostructures embedded in a high-finesse optical microcavity (see Refs. [46,47] and references therein). In our case, however, the excitons—the "matter" part of polaritons—are localized in QDs. The polariton was recently observed in the strong-coupling regime in CQED experiments [42] with gallium-arsenide (GaAs) QDs embedded in a photonic crystal nanocavity. In all these cases, pure exciton and cavity photon states are not the eigenstates of the system. If the system is initialized in one of these states, e.g., by the laser excitation, the system exhibits Rabi oscillations with the characteristic energy of $\hbar g$. Our studies demonstrate that, if such a polariton is formed in two entangled QDs, the entanglement is also transferred to the photon counterpart of the polariton together with the respective population oscillations.

C. Analytical model

There have been several model studies of entanglement in related systems involving qubits coupled to cavities in some fashion [48–51] that can shed some light on the present results. We find the model of Ref. [48] to be particularly helpful. In this model, qubit (or quantum dot) A is coupled to photonic cavity a, and qubit B is coupled to photonic cavity b with no direct coupling between A and B or a and b. As such, eigenstates of the model are easily found and the time evolution of any initial state can be determined analytically. (We do not consider any non-Hermitian contributions corresponding to losses so that, in effect, this model is a strong-coupling limit model.) Of course our case is more complicated with coupling between A and B induced via an additional plasmonic mode. However, the nature of our pulsed excitation model and the coupling of the qubits through the plasmonic modes is such that an antisymmetric entangled state between the qubits is created after a period of time.

With the model of Ref. [48] in mind, we consider our system in the limit of strong photonic cavity–qubit coupling [Fig. 3(b)]. We imagine that an entangled antisymmetric qubit (or quantum dot) state, $|\Psi^-\rangle$, has been generated via the plasmonic coupling. This state may be written as

$$|\Psi^-\rangle = \frac{1}{\sqrt{2}}(-|e_A; g_B\rangle + |g_A; e_B\rangle), \tag{6}$$

where g_A, e_A and g_B, e_B denote ground and excited states of the qubits. (In this discussion it is clearer to use the alphabetical state labeling convention of Ref. [48] as opposed to the numerical one we have used up to this point.) With no photons in the photonic cavities or photonic state $|0_a; 0_b\rangle$, the full system state for this case corresponds to $|\Psi_{00}^-\rangle = |\Psi^-\rangle|0_a; 0_b\rangle$. We further assume that some part of this state has also leaked into the cavity modes. While there are many possible cavity

mode states, the lowest energy one of relevance to photon-pair coincidences is one corresponding to one quantum in cavity mode a and one quantum in cavity mode b, which we denote $|1_a;1_b\rangle$. The full system state corresponding to this case may be written as $|\Psi_{11}^-\rangle = |\Psi^-\rangle|1_a;1_b\rangle$. The time evolution of a superposition of this state with the originally entangled state with no quanta in the cavity modes is given by

$$|\Psi(t)\rangle = \frac{1}{(1+\varepsilon^2)^{1/2}}(|\Psi_{00}^-(t)\rangle + \varepsilon|\Psi_{11}^-(t)\rangle), \tag{7}$$

where the time dependence arises simply from expanding $|\Psi_{00}^-\rangle$ and $|\Psi_{11}^-\rangle$ in terms of the system's eigenstates (Appendix C).

If ε is real and the fraction of $|1_a;1_b\rangle$ photon state is low $\varepsilon \ll 1$ then the dynamics is dominated by $|\Psi_{00}^-(t)\rangle$. In this case, as shown in Ref. [48], the concurrence between the qubits is

$$C_{AB}(t) = \cos^2(gt), \tag{8}$$

where g is the coupling between each qubit and its respective cavity. Furthermore, this concurrence [as we have found in our full calculations with the plasmonic mode coupling, Figs. 3(a) and 4(a)] oscillates between the qubit modes and the photonic cavities. Appendix C gives a more general expression for $C_{AB}(t)$, as well as the corresponding analysis for same-time two-photon correlation function $g_{ab}^{(2)}(t)$. For small but finite ε we show in Appendix C that $g_{ab}^{(2)}(t)$ contains $\sin^4(gt)$ in its denominator, which leads to very strong spikes correlating with high concurrence in the qubits, just as we have also observed in our full system [e.g., Fig. 3(b)].

D. Entanglement storage in high-quality cavity modes

To more fully characterize the effects of coupling with the cavity modes on QD entanglement, we compared the time dependencies for the concurrence $C(t)$ of QDs in the cavities in the strong-coupling regime with that obtained when the cavity modes are absent (an open geometry with $g = 0$). In these simulations, we take the QD decay rates to be [36,52] 50 μeV and 500 μeV and compared the previously obtained results. Our findings are summarized in Fig. 5. It is seen that, since the characteristic decay rate of photon modes in high-quality microcavities with $Q \sim 10^6$ are smaller than the QD nonradiative population relaxation rate, the QD concurrence time decay rate is weaker in the case when the QD-cavity photon mode coupling is present. In other words, the entanglement of QDs in the optical cavities is *stored* in the high-quality subsystem (photons) for a longer time compared to QDs in an open geometry. Specifically, at $\hbar g = 10$ meV, the concurrence of QDs in the cavities is $\approx$4.58$\times$ greater than that in the open geometry at $t = 4814$ fs for the QD relaxation rate of 500 μeV, and is 1.35$\times$ greater at $t = 9027$ fs for $\hbar g = 3$ meV and the QD relaxation rate of 50 μeV, as is seen in the main plot and inset of Fig. 5, respectively. The effective concurrence decay rate is approximated by the following expression:

$$\gamma \approx \alpha_{\mathrm{QD}}\gamma_{\mathrm{QD}} + \alpha_C\gamma_C, \tag{9}$$

where $\alpha_{\mathrm{QD}(C)} = \bar{n}_{\mathrm{QD}(C)}/(\bar{n}_{\mathrm{QD}} + \bar{n}_C)$ is the fraction of time, during which the system occupies the QD (cavity) state,

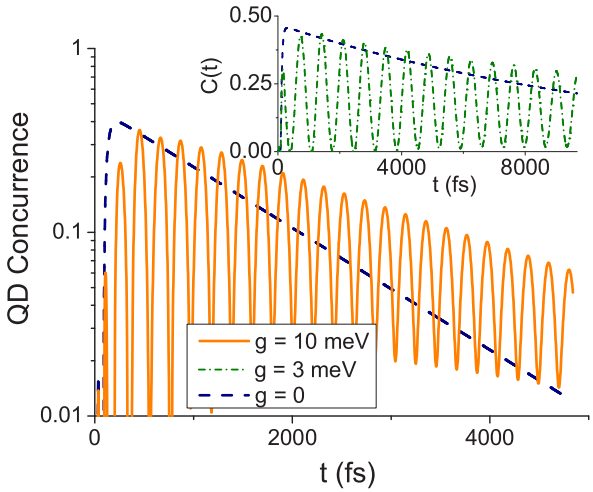

FIG. 5. Storage of the entanglement of QDs in high-finesse cavities in the strong-coupling regime, compared to QDs in an open geometry. As is seen in the main plot, at $t = 4814$ fs, the concurrence of QDs in the cavities is $\approx$4.58$\times$ greater that that with no cavities. The QD decay rates are 500 μeV (main plot) and 50 μeV (inset); the cavities' quality factor is $Q = 10^6$; the photon and QD dephasing rates are 8.6 μeV; the cavity photon energy is $\hbar\omega = 2.05$ eV; the cavity photon decay rate is $Q^{-1}\hbar\omega = 2.05$ μeV [16,17,36,42,52]. The strength of the QD-photon interactions is marked in the plot.

and $\bar{n}_{\mathrm{QD}(C)}$ are the time-averaged occupation numbers for the QD (cavity). Thus, by lowering γ_C (increasing the cavity Q factor), one can decrease the overall concurrence decay rate, as follows from Eq. (9). If the QD and cavity modes are in exact resonance, the occupation time average is $\alpha_{\mathrm{QD}} \approx \alpha_C \approx \frac{1}{2}$ and, thus, one has $\gamma \approx \frac{1}{2}(\gamma_{\mathrm{QD}} + \gamma_C)$. However, under the off-resonant strong-coupling conditions, the average occupation time of the cavity mode can be $\alpha_C > \frac{1}{2}$ if the photonlike polariton is excited by the driving pulse [46]. The latter potentially enables one to further lower the concurrence decay rate.

Finally, we investigated the effect of the pumping pulse duration and of a continuous wave (CW) pump on the entanglement formation of asymmetrically coupled QDs in optical cavities (see Appendix D). We found that during the period of time when the driving pulse is turned on, the QD and photon populations tend to their equilibrium values whereas the QD entanglement does not form in both weak- and strong-coupling regimes. However, the QD concurrence $C > 0$ formed after $\sim$100 fs after the driving pulse is turned off. Therefore, unlike a CW driven system, the free dynamics of the initially excited system could be used to generate and optically detect robust QD entanglement. We also found that setting of the QD-plasmon interaction strength to the same value for both QDs (i.e., where no QD entanglement was formed) resulted in $g_{12}^{(2)}(t) \to 1$ with no photon antibunching observed, as is detailed in Appendix D.

IV. CONCLUSION

In this work, we have shown how to identify entanglement of coupled QD qubits via cavity photon correlation measurements. Specifically, our results could contribute to

quantum simulations that utilize exciton-polariton entangled states [53]. The obtained results may help one to determine, through optical experiments, the exciton and/or photon entangled states [54] revealed in recent experiments with quasi-two-dimensional core-shell nanoplatelets [55]. The conservation of total entanglement we have seen in the strong-coupling limit of the cavity-QD qubit interactions also suggests an alternative means of preserving entanglement.

By considering cavity-photon and QD exciton dynamics coupled with surface plasmons optically excited by a femtosecond laser pulse, we showed that the character of the QD entanglement formation is different in strong- and weak-coupling regimes between the photons and QDs—oscillatory vs slowly decaying entanglement. In both regimes, the same-time pair correlation function $g_{ij}^{(2)}(t)$ of the cavity photons is sensitive to the QD concurrence formation. In particular, in the strong photon-QD coupling regime, $g_{ij}^{(2)}(t)$ peak formation—bunching—correlates with the QD entanglement formation. This can be understood as the effect of the entanglement oscillations between the QD and the cavity photons due to the exciton polariton formation. In the time intervals between the peaks, the photons emitted by the entangled QDs strongly antibunch, $g_{ij}^{(2)}(t) < 0.2$. This behavior contrasts with $g_{ij}^{(2)}(t) \approx 1$ for unentangled QDs, enabling direct optical detection of QD qubit entanglement.

The correlations exhibited in our proposed quantum-dot–photonic-cavity system can seem surprising. For example, often nonclassical (e.g., entangled) states are associated with antibunching or small values of pair correlation function $g^{(2)}$ and this has been shown for plasmon-QD systems [25]. (See, however, different behavior for Gaussian squeezed states [56].) However, keeping in mind we are engineering strong coupling between the photonic modes and the QDs, there is an exchange of entanglement between these subsystems. Thus, when the QDs are nonclassical the photonic modes are not, and vice versa, leading to the photon pair correlation function paralleling the concurrence behavior of the QDs.

To experimentally achieve the solid-state photonic qubit system (Fig. 1) proposed one could use, as quantum dots, the cadmium selenide (CdSe) nanoplatelets of Ref. [55]. While metal nanoparticles represent one avenue for the mode coupling the two QDs, a silicon microdisk resonator supporting a weakly dissipative mode might be more easily used. The two photonic cavity modes could be realized with high-quality photonic crystals composed of silicon nitride, for example. Finally, one can envision optical fibers connected to the two photonic crystals that would lead to photon coincidence detectors for the time-resolved pair correlation function measurements [32,33]. Such an experimental setup would need subpicosecond resolution for the detection of the spikes in the $g^{(2)}$ signal, which has yet to be demonstrated. Alternative physical systems which also demonstrate dissipation-driven entanglement and would have significantly longer time scales, such as plasmonically coupled nitrogen vacancy centers [57], could also be used.

ACKNOWLEDGMENTS

We thank Xuedan Ma for helpful discussions. G.V.K. gratefully acknowledges support from the U.S. Department of Energy, Office of Science, Office of Workforce Development for Teachers and Scientists (WDTS) under the Visiting Faculty Program (VFP). G.V.K. is also grateful to the U.S. Department of Defense for partial support under Contract No. W911NF1810433. This work was performed, in part, at the Center for Nanoscale Materials, a U.S. Department of Energy Office of Science User Facility, and supported by the U.S. Department of Energy, Office of Science, under Contract No. DE-AC02-06CH11357.

APPENDIX A: SIMULATION PARAMETERS

The pulse intensity is characterized by the fluence [16,17,29],

$$F = \int_{-\infty}^{\infty} dt \sqrt{\varepsilon_{\text{med}}} c \varepsilon_0 E^2(t), \tag{A1}$$

where $\varepsilon_{\text{med}} = 2.25$ is the relative dielectric constant of the surrounding polymer matrix, c is the speed of light in vacuum, and ε_0 is the vacuum permittivity. In the simulations, we restricted the number of plasmon (cavity photon) energy levels of the underlying physical system Hamiltonian $\hat{H}_0$ to $N_{\text{ph(pl)}}$ and then numerically integrate Eq. (1) in the main text.

The effect of the electromagnetic interactions of the QD excitons with the damped surface plasmon system in a neighboring metal particle or nanostructure is twofold. First, the asymmetry in the QD-plasmon coupling $\Delta g_s \neq 0$ induces a spontaneously formed entanglement of the QD excitonic states [15,17] with the maximum entanglement achieved at $g_s^1/g_s^2 \approx 1/\sqrt{3}$ [16]. Here, the asymmetry in the QD-plasmon coupling strength is defined as

$$\Delta g_s \equiv g_s^1 - g_s^2, \tag{A2}$$

where the upper index $i = 1, 2$ in g_s^i marks the quantum dots, as defined in the main text.

Second, due to the Purcell effect, the interactions modify the exciton nonradiative decay rate, compared to that in an isolated dot, to $\gamma_{\text{QD}} = 4(g_s)^2/\gamma_s$ [29] (with g_s being the averaged QD-plasmon interaction strength, as defined in the main text). The latter results in the modified effective coupling constant ($\gamma_{\text{QD}} \gg \gamma_C$),

$$\xi = \frac{g\gamma_s}{g_s^2}, \tag{A3}$$

for the symmetric, superradiant exciton states in the coupled QDs. However, the antisymmetric, subradiant collective exciton states are only weakly coupled to the plasmonic system [16] thus, the nonradiative decay γ_{QD} dominates in this case. In the pulsed pumping, the symmetric and antisymmetric states are initially excited, but the symmetric state rapidly decays due to coupling with surface plasmons thus, controlling the fast population damping mechanism in the system. Thus, we characterize our system via the effective coupling constant ξ, as defined in Eq. (A3) above.

APPENDIX B: SYMMETRICALLY COUPLED QUANTUM DOTS

To demonstrate that the formation of the QD entanglement is the key factor influencing the cavity photon correlation

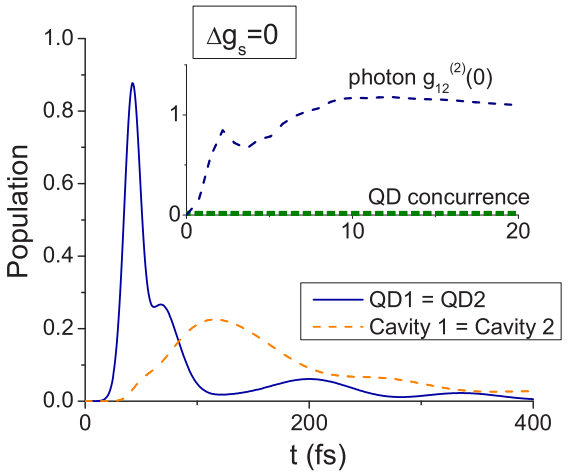

FIG. 6. (a) Population (main plot), QD concurrence, and cavity photon correlations (inset) for equal plasmon coupling $\Delta g^s = 0$. It is seen in the inset that the QD concurrence is $C(t) \ll 1$ and, at the same time, the pair cross-correlation function for the cavity photons tends to $g_{12}^{(2)}(t) \approx 1$ for $t > 10$ fs. The QD-plasmon interaction strength is the same for both dots, $\hbar g_s^1 = \hbar g_s^2 = 30$ meV; $\hbar g = 1$ meV; $\hbar\gamma_s = 150$ meV; the QD decay and dephasing rates are 0.05 μeV and 8.6 μeV; the respective photon decay and dephasing rates are 0.1 meV and 8.6 μeV; the transition dipole moments for the surface plasmons and QDs are $d_s = 4000$ D and $d_i = 13$ D; the energy level spacing of the QD and cavity photon systems is $\hbar\omega = 2.05$ eV.

pattern described above, we studied the dynamics of the system with symmetrically coupled QDs, that is, with $\Delta g_s = 0$. It is known that the concurrence formed in plasmonically coupled QDs is negligible when the coupling values are equivalent [16,17]. Our results obtained for $\xi_{\text{eff}} = 2.68$ are shown in Fig. 6. It is seen that in this case the QD concurrence is $C(t) < 0.06$ in accordance with the existing theory and simulations in Refs. [16,17]. It is also evident from Fig. 6 that the cavity photon cross-correlation function $g_{12}^{(2)}(t)$ rapidly approaches unity.

APPENDIX C: ANALYTICAL MODEL

In this Appendix section, we present the analytical model, which is sketched in Sec. III C of the main text. As is mentioned in the main text, in this part we use the notation of Ref. [48], that is, qubit (or quantum dot) $A(B)$ is coupled to photonic cavitiy $a(b)$. Following the model [48], we consider the case where there is no direct coupling between A and B or a and b. Below we use the following shorthand notations for the states of QD A and cavity a,

$$|0_{Aa}\rangle \equiv |g_A; 0_a\rangle, \tag{C1}$$

$$|1_{Aa}^{\pm}\rangle \equiv \frac{1}{\sqrt{2}}(\pm|e_A; 0_a\rangle + |g_A; 1_a\rangle), \tag{C2}$$

$$|2_{Aa}^{\pm}\rangle \equiv \frac{1}{\sqrt{2}}(\pm|e_A; 1_a\rangle + |g_A; 2_a\rangle), \tag{C3}$$

$$\ldots \tag{C4}$$

$$|n_{Aa}^{\pm}\rangle \equiv \frac{1}{\sqrt{2}}(\pm|e_A; (n-1)_a\rangle + |g_A; n_a\rangle), \tag{C5}$$

and similar notations for the states of QD B and cavity b,

$$|0_{Bb}\rangle \equiv |g_B; 0_b\rangle, \tag{C6}$$

$$|1_{Bb}^{\pm}\rangle \equiv \frac{1}{\sqrt{2}}(\pm|e_B; 0_b\rangle + |g_B; 1_b\rangle), \tag{C7}$$

$$|2_{Bb}^{\pm}\rangle \equiv \frac{1}{\sqrt{2}}(\pm|e_B; 1_b\rangle + |g_B; 2_b\rangle), \tag{C8}$$

$$\ldots \tag{C9}$$

$$|n_{Bb}^{\pm}\rangle \equiv \frac{1}{\sqrt{2}}(\pm|e_B; (n-1)_b\rangle + |g_B; n_b\rangle). \tag{C10}$$

Here $|e_{A(B)}\rangle$ and $|g_{A(B)}\rangle$ are the respective excited and ground states of the QD $A(B)$ and $n_{a(b)} = 0, 1, 2\ldots$ labels the number of quanta in the respective states $a(b)$.

The full system eigenstates are

$$|0_{Aa}, 0_{Bb}\rangle, \quad |0_{Aa}, 1_{Bb}^{-}\rangle, \quad |0_{Aa}, 1_{Bb}^{+}\rangle, \quad |1_{Aa}^{-}, 0_{Bb}\rangle, \quad |1_{Aa}^{+}, 0_{Bb}\rangle, \ldots, \tag{C11}$$

with the energies $\lambda_{a(b)}^{\pm} = n_{a(b)} \pm \sqrt{n_{a(b)}} g_{a(b)}$, where $g_{a(b)}$ are the photon-QD coupling strength in cavity $a(b)$.

In the case where the quantum dots are entangled in an antisymmetric Bell state at $t = 0$,

$$|\Psi^{-}\rangle = \frac{1}{\sqrt{2}}(-|e_A; g_B\rangle + |g_A; e_B\rangle), \tag{C12}$$

and the initial photon population in the cavities are zero, the initial state of the system is

$$|\Psi_{00}^{-}(0)\rangle = |\Psi^{-}\rangle|0_a; 0_b\rangle. \tag{C13}$$

At a later moment of time, the state of the system was determined as a solution of the Schrödinger equation for QD excitons and cavity photons:

$$|\Psi_{00}(t)\rangle = \tfrac{1}{2}[e^{-i(\omega_0 - g)t}(|1_{Aa}^{-}; 0_{Bb}\rangle - |0_{Aa}; 1_{Bb}^{-}\rangle) + e^{-i(\omega_0 + g)t}(|0_{Aa}; 1_{Bb}^{+}\rangle - |1_{Aa}^{+}; 0_{Bb}\rangle)]. \tag{C14}$$

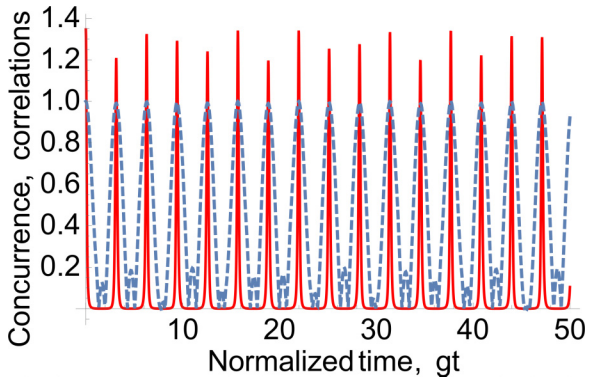

FIG. 7. Normalized correlation function of cavity photons $g_{ab}^{(2)}(t)$, Eq. (C25) [solid (red) curve] and quantum-dot concurrence C, Eq. (C31), analytically calculated for the state $|\Psi(t)\rangle$ given in Eq. (7) at $\varepsilon = 0.1$. In the figure, the correlation function $g_{ab}^{(2)}(t)$ is divided by a factor of 75 for better visibility. It is seen that the peaks at the photon $g_{ab}^{(2)}(t)$ curve are positioned at the same moments of time, at which the QD concurrence reached its maxima, in agreement with the results of our simulations in Fig. 3(a).

Here we suggest that the excitons in QDs A and B are coupled with the cavity modes with the same strength, $g_a = g_b \equiv g$ (as in the main text) and set $\hbar = 1$.

In the case where the initial photon population is one photon per cavity, the initial state of the system is

$$|\Psi_{11}^{-}(0)\rangle = |\Psi^{-}\rangle|1_a; 1_b\rangle. \tag{C15}$$

At a later moment of time, the state of the systems is

$$|\Psi_{11}^{-}(t)\rangle = \frac{1}{2\sqrt{2}} e^{-3i\omega_0 t} \sum_{i=1}^{4} \phi_i e^{-i\lambda_i t}, \tag{C16}$$

where

$$\phi_1 = |1_{Aa}^{+}; 2_{Bb}^{+}\rangle - |2_{Aa}^{+}; 1_{Bb}^{+}\rangle, \tag{C17}$$

$$\phi_2 = |1_{Aa}^{-}; 2_{Bb}^{+}\rangle - |2_{Aa}^{+}; 1_{Bb}^{-}\rangle, \tag{C18}$$

$$\phi_3 = |2_{Aa}^{-}; 1_{Bb}^{+}\rangle - |1_{Aa}^{+}; 2_{Bb}^{-}\rangle, \tag{C19}$$

$$\phi_4 = |2_{Aa}^{-}; 1_{Bb}^{-}\rangle - |1_{Aa}^{-}; 2_{Bb}^{-}\rangle, \tag{C20}$$

and

$$\lambda_1 = (\sqrt{2}+1)g, \quad \lambda_2 = (\sqrt{2}-1)g, \tag{C21}$$

$$\lambda_3 = -(\sqrt{2}-1)g, \quad \lambda_1 = -(\sqrt{2}+1)g. \tag{C22}$$

As it follows from numerical analyses in the main text, at large time the occupation of cavity photon modes is low. In this case, one can approximate the state of the system as a linear combination of wave functions (C14) and (C16); see Eq. (7) in the main text.

We calculated the pair correlation function of cavity photons, as defined in the main text.

For the state vector $|\Psi(t)\rangle$, Eq. (7), the photon population is the following,

$$n_a(t) = n_b(t) \equiv \langle\Psi(t)|\hat{c}_a^{\dagger}\hat{c}_a|\Psi(t)\rangle = \frac{1}{4(\varepsilon^2+1)}[1 + 4\varepsilon^2 - \varepsilon^2\cos(2\sqrt{2}gt) + (\varepsilon^2 - 1)\cos(2gt)]. \tag{C23}$$

The un-normalized photon pair cross-correlation function for photons in the same state is

$$G_{ab}^{(2)}(t) = \langle\Psi(t)|\hat{c}_a^{\dagger}\hat{c}_b^{\dagger}\hat{c}_b\hat{c}_a|\Psi(t)\rangle = \frac{\varepsilon^2}{2(\varepsilon^2+1)}\cos^2(gt)(3 - \cos(2\sqrt{2}gt)). \tag{C24}$$

The normalized correlation function for photons is defined by the usual relation,

$$g_{ab}^{(2)}(t) = \frac{G_{ab}^{(2)}(t)}{n_a(t)n_b(t)}, \tag{C25}$$

where $G_{ab}^{(2)}(t)$, $n_a(t)$, and $n_b(t)$ are defined in Eqs. (C23) and (C24).

For the sake of convenient notations, we number the basis functions of the QDs as follows: $0 = |0, 0\rangle$, $1 = |0, 1\rangle$, $2 = |1, 0\rangle$, $3 = |1, 1\rangle$ where the first (second) index shows the occupation of QD $A(B)$. In these notations, the reduced density matrix of the QDs, ρ_{ij}, in the state (7) has the following nonzero matrix elements:

$$\rho_{00} = \frac{1}{8(\varepsilon^2+1)}\{2\varepsilon^2\cos(2gt) - 2\varepsilon^2\cos[2\sqrt{2}gt] - \varepsilon^2\cos[2(\sqrt{2}-1)gt] - \varepsilon^2\cos[2(1+\sqrt{2})gt] - 4\cos(2gt) + 2\varepsilon^2 + 4\}, \tag{C26}$$

$$\rho_{03} = \rho_{30} = \frac{\varepsilon}{\varepsilon^2+1}\sin^2(gt)\cos(\sqrt{2}gt), \tag{C27}$$

$$\rho_{11} = \rho_{22} = \frac{1}{8(\varepsilon^2+1)}\{\varepsilon^2\cos[2(\sqrt{2}-1)gt] + \varepsilon^2\cos[2(1+\sqrt{2})gt] + 2\cos(2gt) + 2\varepsilon^2 + 2\}, \tag{C28}$$

$$\rho_{12} = \rho_{21} = -\frac{1}{4(\varepsilon^2+1)}\cos^2(gt)[\varepsilon^2\cos(2\sqrt{2}gt) + \varepsilon^2 + 2], \tag{C29}$$

$$\rho_{33} = \varepsilon\rho_{03} = \frac{\varepsilon^2}{\varepsilon^2+1}\sin^2(gt)\cos^2(\sqrt{2}gt). \tag{C30}$$

The Wootters' concurrence [31] of the QDs determined for the density matrix (C26)–(C30) is

$$C = \max(0, \alpha_1 - \alpha_2 - \alpha_3 - \alpha_4), \tag{C31}$$

where α_i $(i = 1...4)$ are the square roots of the eigenvalues of the spin-flipped density matrix,

$$\rho_{11} \pm \rho_{12}, \quad \sqrt{\rho_{00}\rho_{33}} \pm \rho_{13}, \tag{C32}$$

taken in the descending order.

The normalized correlation function of cavity photons $g_{ab}^{(2)}(t)$, and quantum-dot concurrence C, calculated via Eqs. (C25) and (C31) for the state $|\Psi(t)\rangle$, Eq. (7), are shown in Fig. 7. It is seen in the figure that the peaks at the photon $g_{ab}^{(2)}(t)$ curve are positioned at the same moments of time, at which the QD concurrence reached its maximums, in agreement with the results of our simulations in Fig. 3(a).

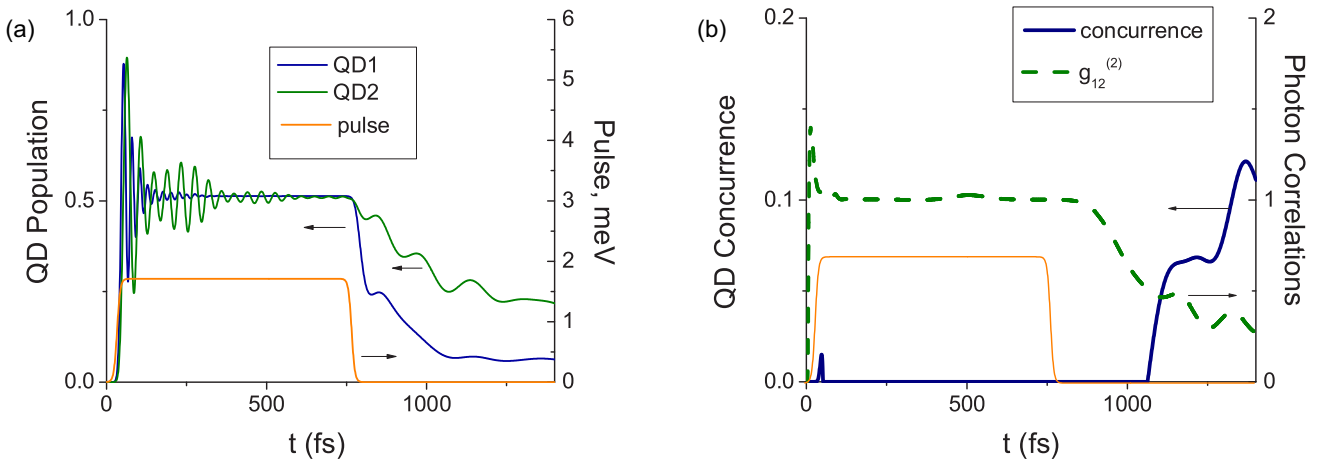

FIG. 8. Quantum dynamics of plasmonically coupled QDs and cavity photons under the action of a long laser pump. The time duration of the laser pulse is $\Delta t = 720$ fs, the characteristic pulse formation, and decay time is $\delta = 10$ fs. The maximum electric field in the pulse is $E_{\max} = 2.5 \times 10^6$ V/m. (a) Population of the first (QD1) and second (QD2) quantum dots as functions of time t (left scale). The orange curve shows the shape of the envelope of the laser pulse $E_0(t)d_i$ where $d_i = 13$ D is the transition dipole moment of QD and $E_0(t)$ is given in Eq. (D1) (right scale). It is seen that after the transient oscillations are damped, the QD populations tend to a steady-state value of 0.5 when the laser pump is turned on and then decrease with time after the pump is turned off. (b) The QD concurrence (left scale) and the cavity photon cross-correlation function $g_{12}^{(2)}$ (right scale). The orange curve shows the laser pulse envelope curve (in arb. units). It is seen that the QD concurrence is $C(t) = 0$ when the pump pulse is on and then begins to increase $\approx$180 fs after the driving pulse is switched off. The photons are emitted with $g_{12}^{(2)} \approx 1$ when the pulse is switched on. The photons antibunch, $g_{12}^{(2)} < 1$, when the QD entanglement is formed after the driving pulse is turned off. In the simulations, the QD-plasmon coupling strength are 30 meV and 17.3 meV for QD1 and QD2, respectively; the QD-photon coupling strength is 10 meV; the plasmon decay rate is 150 meV; the QD decay and dephasing rates are 0.05 μeV and 8.6 μeV, respectively; the respective photon decay and dephasing rates are 0.1 meV and 8.6 μeV; the transition dipole moments for the surface plasmons and QDs are $d_s = 4000$ D and $d_i = 13$ D; the energy level spacing of the QD and cavity photon systems is $\hbar\omega = 2.05$ eV.

At small $\varepsilon \ll 1$, the normalized photon cross-correlation function is

$$g_{ab}^{(2)}(t) = \frac{2\epsilon^2 \cos^2(gt)(3 - \cos(2\sqrt{2}gt))}{\sin^4(gt)}. \tag{C33}$$

To the same approximation, the square roots of the eigenvalues of the spin-flipped density matrix in Eq. (C31) become

$$\tfrac{1}{2}(1 + \cos(2gt)) + \tfrac{1}{8}\epsilon^2\{2\cos[2\sqrt{2}gt]\cos^2(gt) - 2\cos^2(gt) - 2\cos(2gt) + \cos[2(\sqrt{2}-1)gt] + \cos[2(1+\sqrt{2})gt]\}, \tag{C34}$$

$$\tfrac{1}{2}\varepsilon^2 \sin^2(gt)\sin^2(\sqrt{2}gt), \tag{C35}$$

$$\varepsilon\left[\frac{1}{\sqrt{2}}((1 - \cos(2t))\sin^2(t)\cos^2(\sqrt{2}t))^{1/2} - \sin^2(t)\cos(\sqrt{2}t)\right], \tag{C36}$$

$$\varepsilon\left[\frac{1}{\sqrt{2}}((1 - \cos(2t))\sin^2(t)\cos^2(\sqrt{2}t))^{1/2} + \sin^2(t)\cos(\sqrt{2}t)\right]. \tag{C37}$$

APPENDIX D: CONTINUOUS WAVE PUMPING

To study the effect of the CW pumping on the system dynamics, we simulate the quantum dynamics of the system under very long laser pulse durations up to 700 fs. In these simulations, the semiclassical electric field of the laser pump is taken to be $E(t) = E_0(t)\cos(\omega t)$ with the envelope function,

$$E_0(t) = E_{\max}\frac{(\tanh[(t_c - t_0)/\delta] + 1)^{-1} + (\tanh[(t_1 - t_c)/\delta] + 1)^{-1}}{(\tanh[(t - t_0)/\delta] + 1)^{-1} + (\tanh[(t_1 - t)/\delta] + 1)^{-1}}, \tag{D1}$$

where $E_{\max}$ is the maximum value of the electric field in the pulse, and $t_c = \frac{1}{2}(t_1 - t_0)$ marks the middle of the time domain where the pulse is applied. For the pulse duration $\Delta t \equiv t_1 - t_0 = 20$ fs and width $\delta = 10$ fs, the pulse (D1) approximates the Gaussian pulse that we used in the main text.

Here we vary the pulse duration Δt from 20 fs to 720 fs. In all simulations, we observe that within the time domain where the pulse is applied, $t_0 - \delta < t < t_1 + \delta$, the QD concurrence is equal to zero, and the cavity photon correlation function was $g_{12}^{(2)} \approx 1$. A typical output of the simulations is shown in

Fig. 8. We also find that approximately 100–300 fs after the pulse is switched off, the entanglement of the QD states occurs [Fig. 8(b)]. At the same time, the photon correlation function is decreased, $g_{12}^{(2)} < 1$, which further confirms our conclusion about the photon antibunching in states with entangled QDs.

We did not observe formation of the QD entanglement within the time domain $t_0 - \delta < t < t_1 + \delta$ when the pulse is turned on. Thus, we infer that the presence of the external CW laser pumping destroys the entanglement in the system and, at the same time, results in virtually coherent emission of cavity photons by the QDs with $g_{12}^{(2)} \approx 1$. This conclusion is in qualitative agreement with the results of existing numerical and analytic analyses of the plasmonically coupled QD dynamics in Ref. [17].

[1] N. Gisin and R. Thew, Quantum communication, Nat. Photonics **1**, 165 (2007).

[2] O. Thearle, J. Janousek, S. Armstrong, S. Hosseini, M. Schünemann (Mraz), S. Assad, T. Symul, M. R. James, E. Huntington, T. C. Ralph, and P. K. Lam, Violation of Bell's Inequality Using Continuous Variable Measurements, Phys. Rev. Lett. **120**, 040406 (2018).

[3] I. Buluta and F. Nori, Quantum simulators, Science **326**, 108 (2009).

[4] S.-K. Liao, W.-Q. Cai, W.-Y. Liu, L. Zhang, Y. Li, J.-G. Ren, J. Yin, Q. Shen, Y. Cao, Z.-P. Li, F.-Z. Li, X.-W. Chen, L.-H. Sun, J.-J. Jia, J.-C. Wu, X.-J. Jiang, J.-F. Wang, Y.-M. Huang, Q. Wang, Y.-L. Zhou, L. Deng, T. Xi, L. Ma, T. Hu, Q. Zhang, Y.-A. Chen, N.-L. Liu, X.-B. Wang, Z.-C. Zhu, C.-Y. Lu, R. Shu, C.-Z. Peng, J.-Y. Wang, and J.-W. Pan, Satellite-to-ground quantum key distribution, Nature (London) **549**, 43 (2017).

[5] T. Schmitt-Manderbach, H. Weier, M. Fürst, R. Ursin, F. Tiefenbacher, T. Scheidl, J. Perdigues, Z. Sodnik, C. Kurtsiefer, J. G. Rarity, A. Zeilinger, and H. Weinfurter, Experimental Demonstration of Free-Space Decoy-State Quantum Key Distribution Over 144 km, Phys. Rev. Lett. **98**, 010504 (2007).

[6] C. Varnava, R. M. Stevenson, J. Nilsson, J. Skiba-Szymanska, B. Dzurňák, M. Lucamarini, R. V. Penty, I. Farrer, D. A. Ritchie, and A. J. Shields, An entangled-LED-driven quantum relay over 1 km, npj Quant. Inform. **2**, 16006 (2016).

[7] IBM Q, an industry-first initiative to build commercially available universal quantum computers for business and science, https://www.research.ibm.com/ibm-q/ (2017).

[8] D. J Reilly, Engineering the quantum-classical interface of solid-state qubits, npj Quant. Inform. **1**, 15011 (2015).

[9] J.-W. Pan, Z.-B. Chen, C.-Y. Lu, H. Weinfurter, A. Zeilinger, and M. Żukowski, Multiphoton entanglement and interferometry, Rev. Mod. Phys. **84**, 777 (2012).

[10] K. M. O'Connor and W. K. Wootters, Entangled rings, Phys. Rev. A **63**, 052302 (2001).

[11] Y.-L. Hua, Z.-Q. Zhou, X. Liu, T.-S. Yang, Z.-F. Li, P.-Y. Li, G. Chen, X.-Y. Xu, J.-S. Tang, J.-S. Xu, C.-F. Li, and G.-C. Guo, Annual-ring-type quasi-phase-matching crystal for generation of narrowband high-dimensional entanglement, Phys. Rev. A **97**, 013836 (2018).

[12] R. H. Dicke, Coherence in spontaneous radiation processes, Phys. Rev. **93**, 99 (1954).

[13] Z. Ficek and R. Tanaś, Entangled states and collective nonclassical effects in two-atom systems, Phys. Rep. **372**, 369 (2002).

[14] D. Martin-Cano, A. Gonzalez-Tudela, L. Martin-Moreno, F. J. Garcia-Vidal, C. Tejedor, and E. Moreno, Dissipation-driven generation of two-qubit entanglement mediated by plasmonic waveguides, Phys. Rev. B **84**, 235306 (2011).

[15] J. Hou, K. Słowik, F. Lederer, and C. Rockstuhl, Dissipation-driven entanglement between qubits mediated by plasmonic nanoantennas, Phys. Rev. B **89**, 235413 (2014).

[16] M. Otten, R. A. Shah, N. F. Scherer, M. Min, M. Pelton, and S. K. Gray, Entanglement of two, three, or four plasmonically coupled quantum dots, Phys. Rev. B **92**, 125432 (2015).

[17] M. Otten, J. Larson, M. Min, S. M. Wild, M. Pelton, and S. K. Gray, Origins and optimization of entanglement in plasmonically coupled quantum dots, Phys. Rev. A **94**, 022312 (2016).

[18] B. Thorgrimsson, D. Kim, Y.-C. Yang, L. W. Smith, C. B. Simmons, D. R. Ward, R. H. Foote, J. Corrigan, D. E. Savage, M. G. Lagally, M. Friesen, S. N. Coppersmith, and M. A. Eriksson, Extending the coherence of a quantum dot hybrid qubit, npj Quant. Inform. **3**, 32 (2017).

[19] X. Hu and S. Das Sarma, Hilbert-space structure of a solid-state quantum computer: Two-electron states of a double-quantum-dot artificial molecule, Phys. Rev. A **61**, 062301 (2000).

[20] T. D. Ladd, F. Jelezko, R. Laflamme, Y. Nakamura, C. Monroe, and J. L. O'Brien, Quantum computers, Nature (London) **464**, 45 (2010).

[21] H. Jayakumar, A. Predojević, T. Kauten, T. Huber, G. S. Solomon, and G. Weihs, Time-bin entangled photons from a quantum dot, Nat. Commun. **5**, 4251 (2014).

[22] G. Burkard, D. Loss, and D. P. DiVincenzo, Coupled quantum dots as quantum gates, Phys. Rev. B **59**, 2070 (1999).

[23] A. Blais, R.-S. Huang, A. Wallraff, S. M. Girvin, and R. J. Schoelkopf, Cavity quantum electrodynamics for superconducting electrical circuits: An architecture for quantum computation, Phys. Rev. A **69**, 062320 (2004).

[24] T. F. Watson, S. G. J. Philips, E. Kawakami, D. R. Ward, P. Scarlino, M. Veldhorst, D. E. Savage, M. G. Lagally, M. Friesen, S. N. Coppersmith, M. A. Eriksson, and L. M. K. Vandersypen, A programmable two-qubit quantum processor in silicon, Nature (London) **555**, 633 (2018).

[25] E. Dumitrescu and B. Lawrie, Antibunching dynamics of plasmonically mediated entanglement generation, Phys. Rev. A **96**, 053826 (2017).

[26] C. Gies, F. Jahnke, and W. W. Chow, Photon antibunching from few quantum dots in a cavity, Phys. Rev. A **91**, 061804 (2015).

[27] N. Thakkar, C. Cherqui, and D. J. Masiello, Quantum beats from entangled localized surface plasmons, ACS Photonics **2**, 157 (2014).

[28] L. Garziano, A. Ridolfo, S. De Liberato, and S. Savasta, Cavity QED in the ultrastrong coupling regime: Photon bunching from the emission of individual dressed qubits, ACS Photonics **4**, 2345 (2017).

[29] R. A. Shah, N. F. Scherer, M. Pelton, and S. K. Gray, Ultrafast reversal of a Fano resonance in a plasmon-exciton system, Phys. Rev. B **88**, 075411 (2013).

[30] M. Otten, QuaC: Open quantum systems in C, a time-dependent open quantum systems solver, https://github.com/0tt3r/QuaC (2017).
[31] W. K. Wootters, Entanglement of Formation of an Arbitrary State of Two Qubits, Phys. Rev. Lett. **80**, 2245 (1998).
[32] Y. Yamamoto and A. Imamoğlu, *Mesoscopic Quantum Optics* (John Wiley & Sons, New York, 1999).
[33] M. O. Scully and M. S. Zubairy, *Quantum Optics* (Cambridge University Press, Cambridge, 1997).
[34] A. Verger, C. Ciuti, and I. Carusotto, Polariton quantum blockade in a photonic dot, Phys. Rev. B **73**, 193306 (2006).
[35] T. Galfsky, J. Gu, E. E. Narimanov, and V. M. Menon, Photonic hypercrystals for control of light–matter interactions, Proc. Natl. Acad. Sci. USA **114**, 5125 (2017).
[36] P. Senellart and I. Robert-Philip, Cavity quantum electrodynamics with semiconductor quantum dots, in *Handbook of Self Assembled Semiconductor Nanostructures for Novel Devices in Photonics and Electronics*, edited by M. Henini (Elsevier, Amsterdam, 2008), pp. 132–164.
[37] M. Pelton, Modified spontaneous emission in nanophotonic structures, Nat. Photonics **9**, 427 (2015).
[38] R. Chikkaraddy, B. de Nijs, F. Benz, S. J. Barrow, O. A. Scherman, E. Rosta, A. Demetriadou, P. Fox, O. Hess, and J. J. Baumberg, Single-molecule strong coupling at room temperature in plasmonic nanocavities, Nature (London) **535**, 127 (2016).
[39] H. N. S. Krishnamoorthy, Z. Jacob, E. Narimanov, I. Kretzschmar, and V. M. Menon, Topological transitions in metamaterials, Science **336**, 205 (2012).
[40] V. Savona, L. C. Andreani, P. Schwendimann, and A. Quattropani, Quantum well excitons in semiconductor microcavities: Unified treatment of weak and strong coupling regimes, Solid State Commun. **93**, 733 (1995).
[41] C. Creatore and A. L. Ivanov, Strong and weak coupling limits in optics of quantum well excitons, Phys. Rev. B **77**, 075324 (2008).
[42] K. Hennessy, A. Badolato, M. Winger, D. Gerace, M. Atatüre, S. Gulde, S. Fält, E. L. Hu, and A. Imamoğlu, Quantum nature of a strongly coupled single quantum dot–cavity system, Nature (London) **445**, 896 (2007).
[43] A. Boca, R. Miller, K. M. Birnbaum, A. D. Boozer, J. McKeever, and H. J. Kimble, Observation of the Vacuum Rabi Spectrum for One Trapped Atom, Phys. Rev. Lett. **93**, 233603 (2004).
[44] E. M. Purcell, H. C. Torrey, and R. V. Pound, Resonance absorption by nuclear magnetic moments in a solid, Phys. Rev. **69**, 37 (1946).
[45] F. Armata, G. Calajo, T. Jaako, M. S. Kim, and P. Rabl, Harvesting Multiqubit Entanglement from Ultrastrong Interactions in Circuit Quantum Electrodynamics, Phys. Rev. Lett. **119**, 183602 (2017).
[46] I. Carusotto and C. Ciuti, Quantum fluids of light, Rev. Mod. Phys. **85**, 299 (2013).
[47] N. S. Voronova, A. A. Elistratov, and Y. E. Lozovik, Detuning-Controlled Internal Oscillations in an Exciton-Polariton Condensate, Phys. Rev. Lett. **115**, 186402 (2015).
[48] M. Yönaç, T. Yu, and J. H. Eberly, Pairwise concurrence dynamics: A four-qubit model, J. Phys. B: At. Mol. Opt. Phys. **40**, S45 (2007).
[49] W. Shu and T. Yu, Exact coherence dynamics mediated by a small environment, J. Phys. B: At. Mol. Opt. Phys. **44**, 225501 (2011).
[50] Y.-L. Dong, S.-Q. Zhu, and W.-L. You, Quantum-state transmission in a cavity array via two-photon exchange, Phys. Rev. A **85**, 023833 (2012).
[51] Y. Rong-Can, Z. Peng-Fei, G. Yan-Qiang, and Z. Tian-Cai, Quantum entanglement dynamics of two atoms in two coupled cavities, Commun. Theor. Phys. **57**, 195 (2012).
[52] K. E. Knowles, E. A. McArthur, and E. A. Weiss, A multi-timescale map of radiative and nonradiative decay pathways for excitons in CdSe quantum dots, ACS Nano **5**, 2026 (2011).
[53] D. G. Angelakis (Ed.), in *Quantum Simulations with Photons and Polaritons*, Quantum Science and Technology (Springer, Cham, 2017).
[54] O. Benson, C. Santori, M. Pelton, and Y. Yamamoto, Regulated and Entangled Photons from a Single Quantum Dot, Phys. Rev. Lett. **84**, 2513 (2000).
[55] X. Ma, B. T. Diroll, W. Cho, I. Fedin, R. D. Schaller, D. V. Talapin, S. K. Gray, G. P. Wiederrecht, and D. J. Gosztola, Size-dependent biexciton quantum yields and carrier dynamics of quasi-two-dimensional core/shell nanoplatelets, ACS Nano **11**, 9119 (2017).
[56] M. Stobinska and K. Wodkiewicz, Witnessing entanglement with second-order correlations, Phys. Rev. A **71**, 032304 (2005).
[57] Wan-li Yang, Jun-Hong An, Cheng-jie Zhang, Chang-yong Chen, and C. H. Oh, Dynamics of quantum correlation between separated nitrogen-vacancy centers embedded in plasmonic waveguide, Sci. Rep. **5**, 15513 (2015).